Article

Cavitation Erosion Resistance and Wear Mechanism Model of Flame-Sprayed Al_2O_3–40%TiO_2/NiMoAl Cermet Coatings

Mirosław Szala[1,*] and Tadeusz Hejwowski[1]

[1] Lublin University of Technology, Faculty of Mechanical Engineering, Department of Materials Engineering, Nadbystrzycka 36D, 20-618 Lublin, Poland; m.szala@pollub.pl (M. Sz.); t.hejwowski@pollub.pl (T. H.)

* Correspondence: m.szala@pollub.pl; Tel.: +48-815-384-209

Abstract: This manuscript deals with the cavitation erosion resistance of low-velocity oxy-flame (LVOF) sprayed Al_2O_3–40%TiO_2/NiMoAl cermet coatings, a new functional application of cermet coatings. The aim of the study was to investigate the cavitation erosion mechanism and determine the effect of feedstock powder ratio (Al_2O_3–TiO_2/NiMoAl) of LOVF cermet coatings on their cavitation erosion resistance. As-sprayed coatings were investigated for roughness, porosity, hardness, Young's modulus. Microstructural characteristics of the cross-section and the surface of as-sprayed coatings were examined by light optical microscopy (LOM) and scanning electron microscopy (SEM) equipped with the EDS and XRD methods. Coatings cavitation tests were conducted in accordance with the ASTM G32 standard with usage of reference samples made from steel, copper and aluminum alloys. Cavitation erosion resistance was measured by weight and volume loss, and normalised cavitation erosion resistance was calculated. Surface eroded due to cavitation was examined in successive time intervals by LOM and SEM-EDS. On the basis of coating properties and cavitation investigations, a phenomenological model of the cavitation erosion of Al_2O_3–40%TiO_2/NiMoAl cermet coatings was elaborated. General relationships between their properties, microstructure and cavitation wear resistance were established. The Al_2O_3–40%TiO_2/NiAlMo composite coating containing 80% of ceramic powder has a higher cavitation erosion resistance than the reference aluminium alloy.

Keywords: cermet coating; aluminia-titania; thermal spraying; cavitation erosion; microstructure; wear model.

1. Introduction

Aluminia-titania sprayed coatings, Al_2O_3–TiO_2, are used in the chemical engineering, metal and paper industries to improve the resistance to wear, corrosion and high temperature oxidation [1–6]. The protective Al_2O_3–TiO_2 ceramic coatings are mainly deposited with 3% [5,7,8], 13% [1,3,8–10], 20% [3], 40% [2,3] or 50% [11] addition of TiO_2. Apart from the fact that plasma spraying (PS) is the most widely used technique of Al_2O_3–TiO_2 ceramic deposition [3,7,8,11,12], processes like low-velocity oxy-fuel (LVOF) [2,5,6], high-velocity oxy-fuel (HVOF) [12] or even laser cladding [1] are also employed. Among the above processes, LVOF spraying is a low power consuming and thus cost-effective method, when compared to other thermal spraying techniques [2,9]. In addition, the Al_2O_3 TiO_2 sprayed coating structure produced by PS of HVOF [13,14] is well-described in the literature. However, data about the microstructure and properties of aluminia-titania coatings deposited by LVOF are rarely reported [15]. In industrial applications different metallic bond coats such as NiAl, NiCr, NiCrAl, NiMoAl or NiCrMo are employed to increase ceramic coating adhesion to the substrate [4,8,14,16]. Coatings deposited with NiMoAl feedstock powders are described in the literature as promoting high bonding strength, good anti-oxidation ability, excellent corrosion and wear resistance, and are widely used as protective coating for many industrial components under high temperature conditions [17]. On the whole, functional properties of both ceramic Al_2O_3–TiO_2 and metallic NiMoAl coatings are complementary, and it seems justified to manufacture composite coating deposited by LVOF that combine the beneficial properties of Al_2O_3–TiO_2 and NiMoAl coatings. Nevertheless, the influence of the microstructure of cermet coatings flame-sprayed with a blend of Al_2O_3–TiO_2 and NiMoAl feedstock powders on their cavitation erosion resistance has not been reported.

Results of the cavitation erosion of various sprayed coatings (WC-Co, CrC or NiAl coatings) are usually reported in reference to bulk metal alloys [18,19], a survey of the literature of the subject indicates that the cavitation erosion resistance (CER) of aluminia-titania ceramics manufactured by LOVF has been inadequately examined. The literature offers the studies of coatings with 13% TiO_2 addition fabricated only by PS or HVOF [10,12] , and the results are usually presented without using any reference bulk metals [12]. As a result, it is difficult to interpret the results and examine the applications for Al_2O_3–TiO_2 coatings. Moreover, the literature survey reveals that only few studies focus on the microstructure and wear resistance properties of cermet coatings, e.g. Cr_3C_2-NiCr/Ni [20], WC-Co/Cr–NiCrFeBSiC [21] and Al_2O_3–TiO_2/NiMoAl [15] cermet coatings, nevertheless the cavitation erosion resistance of LVOF-sprayed Al_2O_3–TiO_2/NiMoAl composite coatings has not been identified, hence it seems worth investigating new functional applications of these coatings. Additionally, it seems worth determining the content ratio of metallic (NiMoAl) to ceramic feedstock powder (Al_2O_3–40%TiO_2) that will ensure the deposition of composite coating Al_2O_3 40%TiO_2/NiMoAl with potentially beneficial CER properties.

This manuscript investigates the cavitation erosion resistance and properties of flame-sprayed Al_2O_3–40%TiO_2/NiMoAl cermet coatings. Deposited coatings have never been examined in relation to their cavitation erosion resistance. The study verifies a new solution for cavitation wear prevention. The aim of the work is to assess the cavitation erosion resistance and wear mechanism of flame-sprayed Al_2O_3–40%TiO_2/NiMoAl cermet coatings as well as to determine the effect of feedstock powder ratios (Al_2O_3–TiO_2/NiMoAl) of flame sprayed (LVOF) composite coatings on cavitation erosion resistance.

2. Material and methods

2.1. Coating manufacturing

The object of our investigation were cermet coatings (Al_2O_3–40%TiO_2/NiMoAl) sprayed with the LVOF method with different weight fractions of ceramic powder (%cp) and metallic powder (%mp). Properties of the metallic powder (mp) and the ceramic power (cp) are given in **Tab. 1**. According to manufacturer's data, the AMI 3452.6 (NiMoAl) powder is intended to be used as bond coat. While the MX 6-3018 (Al_2O_3-40%TiO_2) powder is applicable for low roughness and high resistance to wear

coatings used in the textile industry or for preventing the wear of pomp seals. The powders vary in grain size and morphology, as described in **Tab. 1** and **Fig 1**.

Tab. 1 Feedstock powder materials

Type of powder (description)	Powder grade	Nominal chemical composition [wt.%]	Grain size [μm]
Metallic powder (mp)	AMI 3452.6	Al=5.2%; Mo=4.9%; Fe=0.8%; Si=0.4%, Ni-bal.	-125+45
Ceramic powder (cp)	MX 6-3018.2	Al_2O_3-40%TiO_2	-40+15

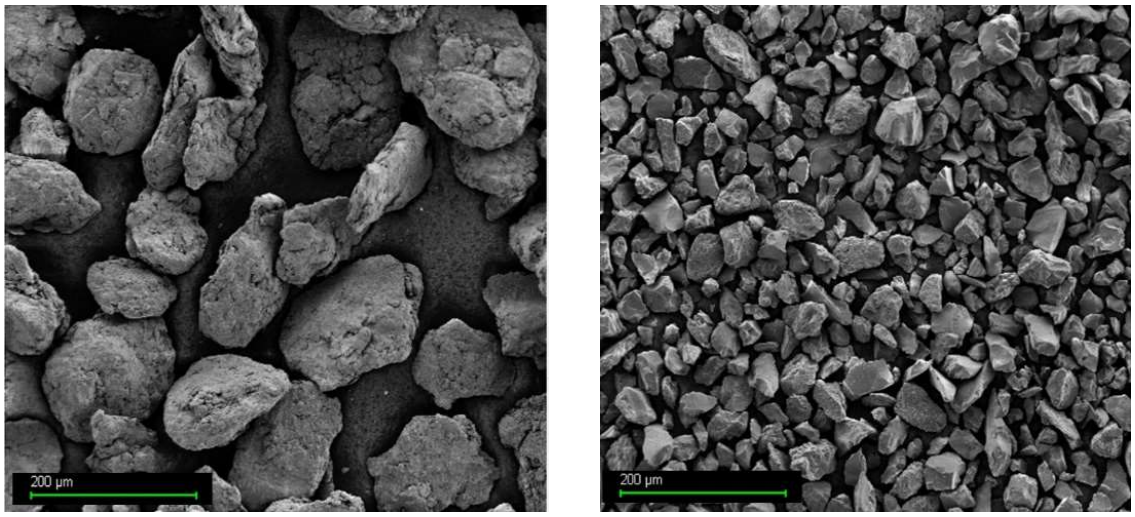

(a) (b)

Fig 1 Fedstock powders: (a) metallic powder - NiMoAl, (b) ceramic powder - Al_2O_3-40%TiO_2, SEM.

Coatings were LVOF (low velocity oxy fuel) sprayed by means of the UTP Uni-Spray-Jet torch (UTP, Bad Kronzingen, Germany). Feedstock powders were delivered to the torch in the argon stream from the feeding station, in which the powder material was kept in fluidized condition [22]. Coatings were deposited on the face of ϕ25x55 mm cylinders made of mild steel grade S235JR (C=0.23%). The deposition parameters were: nozzle - S, oxygen pressure - 0.3 MPa, acetylene pressure - 0.07 MPa, standoff distance - 180 mm. Prior to spraying, the steel substrate was sand blasted with 70 mesh corundum to Ra=15.2 μm. Eleven steel coupons were deposited with different types of coating system. The first coupon was sprayed only with NiMoAl metallic powder (mp) and the coating thickness of about 250 μm. Other ten substrates were sprayed with mp bond coats of approximately 100 μm thickness and then sprayed with different cermet top layers. Nine top coats were deposited with the blends of mp and cp (Al_2O_3–40%TiO_2 and NiMoAl powders) sprayed with a gradual addition of 10% ceramic powder ranging from 10% to 90% of cp. Each subsequent cermet sample was produced with a 10% higher content of the ceramic powder than the previous. 100%cp top layer was deposited onto the last bond coat. The thickness of the top coats was about 200 μm.

2.2 Characterization techniques

As-sprayed coatings were examined for hardness, microstructure and phase composition with light optical microscopy (LOM), scanning electron microscopy with energy-dispersive X-ray spectroscopy (SEM-EDS) and phase X-ray diffraction (XRD). The composite structure of Al_2O_3-TiO_2/NiMoAl coatings was studied on the cross-section by means of LOM (Nikon MA200). The porosity of sprayed coatings was measured with the ImagePro computer image analysis software and ten photos per sample were evaluated. Nanohardness measurements were conducted by means of a nanoindentation tester (CSM Instruments) with a load of 150 mn and a dwelling time of 10 s. Elastic modulus calculations were based on a modified Oliver and Pharr approach with Poisson's

ratio set equal to 0.3. The coating were examined by the X-ray diffraction measurement method (XRD) using a Philips PW1850 diffractometer (Eindhoven, The Netherlands) with Cu-Kα radiation. As-sprayed coating surface morphology was investigated with both the SEM-EDS method using (Phenom World Pro-X) and surface profilometer methods. The Surtronic tester profilometer (Taylor Hobson, U.K.) was used to measure surface roughness of the samples. The coating average surface roughness parameter (Ra) value was defined according to the ISO standard.

2.3 Cavitation erosion testing

A set of as-sprayed Al_2O_3–40%TiO_2 /NiMoAl coating specimens with the dimensions of ϕ25x5 mm was machined from sprayed cylinders and then subjected to cavitation tests. According to the literature-cited data on cavitation erosion, steels, copper and aluminium alloys are usually used as standard reference materials. Hence, in our experiment, the reference coupons were manufactured from these structural alloys, as presented in **Tab. 2**. This will facilitate a comparison of results obtained for the sprayed Al_2O_3–40%TiO_2/NiMoAl coatings with the cavitation erosion data given in the literature [18,19,23,24].

Tab. 2 Reference samples used in cavitation erosion tests

Sample code	Grade	Main chemical element composition [wt.%]
AlSi	AlSi7Mg	Al-base; Si-7.5%; Mg-6.5%
CuZn	CuZn40Pb2	Cu-base; Zn-40%; Pb-2%
FeC	C45	Fe-base; C-0.45%

The cavitation tests were conducted on an ultrasonic test stand in accordance with the ASTM G-32 [25] standard recommendations. The stationary specimen method was employed, in which the gap between horn tip and test surface was set equal to 1 mm, the amplitude and frequency of the tests were 50 μm and 20 kHz, respectively. Distilled water was used as a cavitation test medium. The water temperature was stabilised at 25 °C. The sonotrode tip diameter was 22 mm. The weight of the samples was measured before and during the test at regular intervals in order to determine cavitation erosion curves. The weight decrease of the samples was periodically estimated at specified time intervals with a 0.1 mg accuracy balance. After 15 minutes of cavitation, normalised cavitation erosion wear (Ne) was calculated by dividing the measured volume of reference material decrease with the volume decrease of the coated samples, both tested under the same test conditions. The reference bulk metal alloy surface was prepared with the Ra roughness parameter lower than 0.08 μm, the coated specimens were investigated in as-sprayed conditions.

The cavitation-worn surface of the samples was assessed during time intervals of the cavitation test with SEM-EDS and optical microscopy using a stereoscope microscope Nikon SMZ 1500. Results of coating microstructural analysis and systematic cavitation-worn surface observations led to elaboration of an innovative phenomenological model of cavitation erosion for Al_2O_3-40%TiO_2/NiMoAl composite coatings.

3. Results and discussion

3.1 Microstructure and properties

The literature survey offers data about the properties of Al_2O_3–TiO_2 –sprayed top coatings. However, there are very few studies providing information about composite coatings deposited by LVOF with the blend of Al_2O_3–40%TiO_2 and NiMoAl powders [15]. In present study, manufactured composite Al_2O_3-40%TiO_2/NiMoAl coating morphology was investigated in cross-section and surface of coatings, **Fig 2** and **Fig 3**, respectively. The general microstructure of a cermet coating is presented in **Fig 2**. The coating consists of a bonding layer (metallic) and a cermet layer (metallic-ceramic) which

Preprints (www.preprints.org) | NOT PEER-REVIEWED | Posted: 6 June 2018 doi:10.20944/preprints201806.0090.v1

Peer-reviewed version available at Coatings 2018, 8, 254; doi:10.3390/coatings8070254

is deposited with different blends of ceramic and metallic powders. The bonding layer acts as a buffer to reduce the thermal stress originating during deposition from cooling to ambient temperature. The coating structures differ with respect to the amount of ceramic splats. It is visible in the microstructure cross-section (**Fig 2**) and the coating surfaces (**Fig 3**) that the amounts of ceramic lamellas and splats increase with the addition of cp portion ranging from 10%cp to 100%cp.

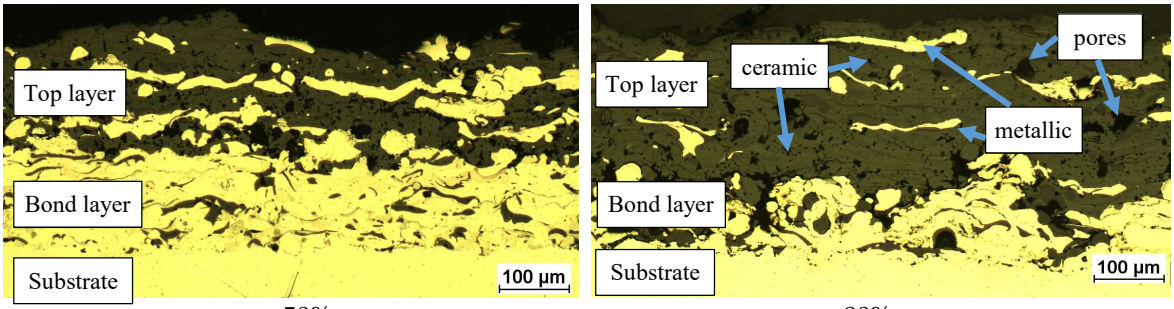

50%cp 80%cp

Fig 2 Microstructure of the coatings deposited with the addition of 50% and 80% of cp (ceramic powder)

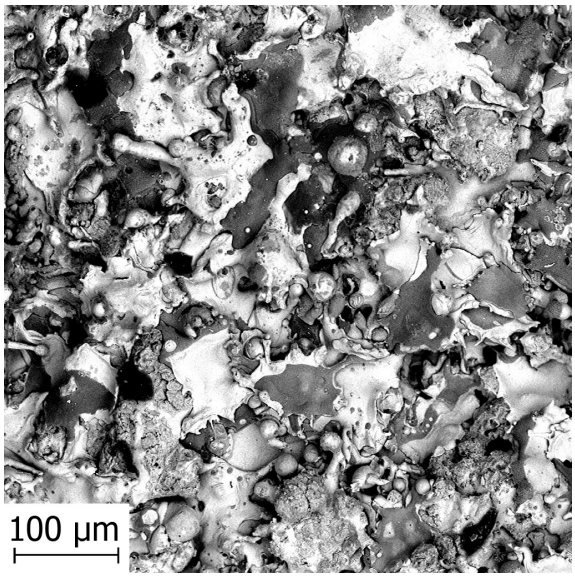

0%cp

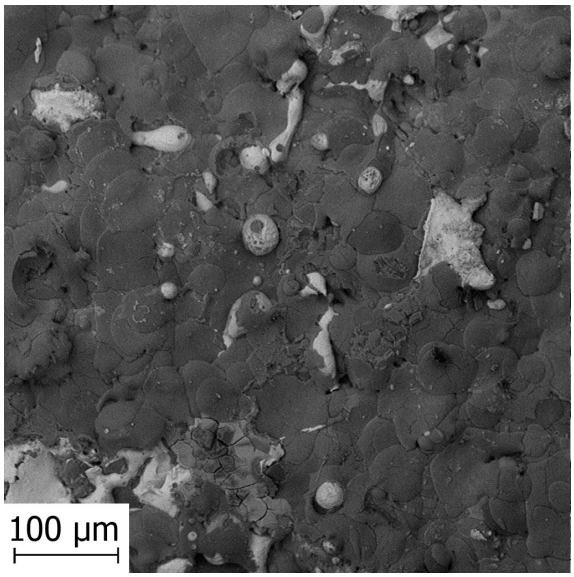

80%cp

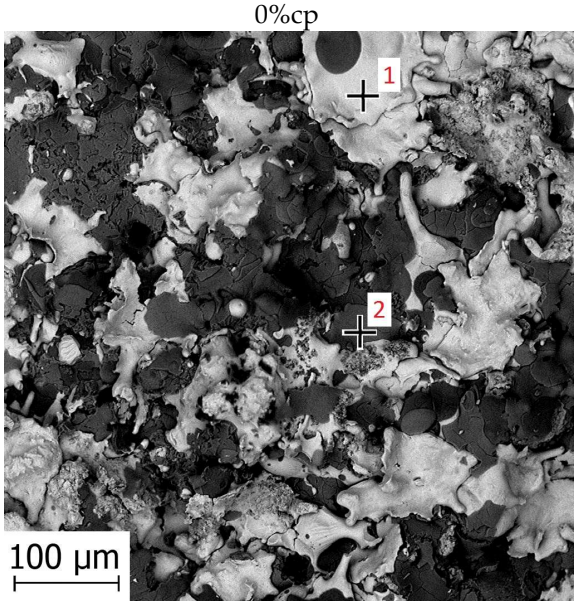

30%cp

Element concentration [wt.%] in 30%cp, SEM-EDS

	Ni	Mo	Al	Ti	O
1.	68.1±1.9	5.1±6.4	9.4±3.9	3.9±5.1	13.1±3.9
2.			26.7±1.9	45.2±3.2	28.9±2.3

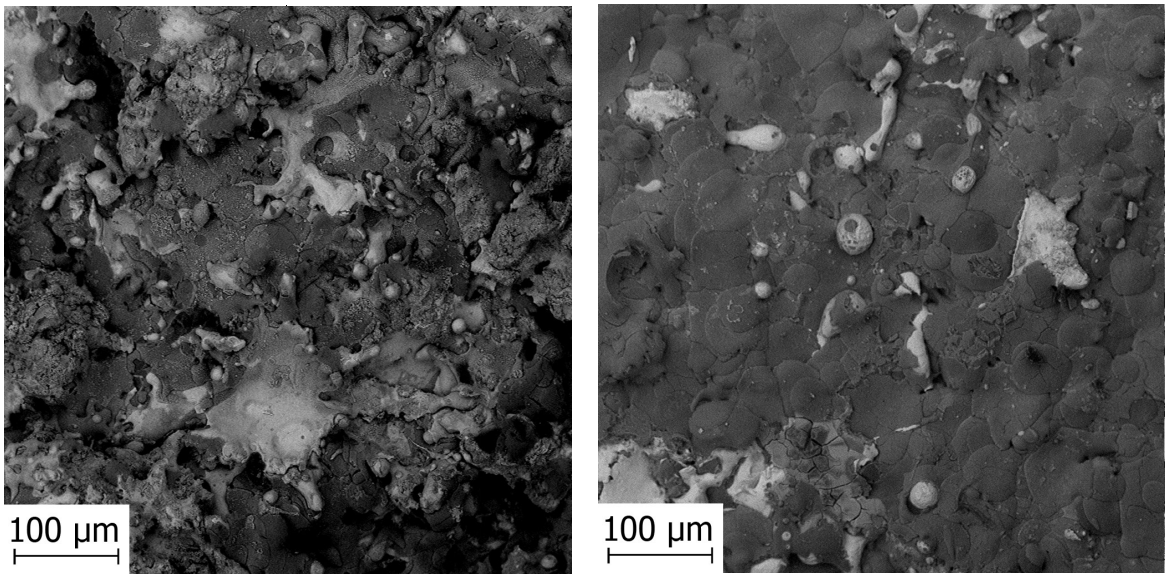

Fig 3. SEM images of coatings as-sprayed with (a) 0%cp, (b) 30%cp, (c) 60%cp, (d) 80%cp, (e) 100%cp at high magnification and the results of 30%cp splats chemical analysis, SEM-EDS

The two-phase cermet top layer consists of ceramic and metallic lamellas derived from ceramic Al_2O_3–40%TiO_2 and metallic NiMoAl feedstock powders. Based on the microscopic observations shown in **Fig 2** and **Fig 3**, it is possible to indicate a typical lamellar microstructure of sprayed coatings [12,26] consisting of metal oxide particles, porosity and partly melted or unmelted particles, which results in an uneven surface with micro-cracks in the ceramic phase. This network of microcracks is caused by the quenching stresses during the cooling of the ceramic lamella. Cracks in the ceramic phase are an inherent phenomenon occurring at the LVOF deposition of ceramic particles [4]. However, the coating cross-section shows no presence of cracks penetrating through the coating thickness, which could negatively influence the coating wear properties. Results of the chemical composition spot analysis (**Fig 3**) reveals that the brighter splats were sprayed with the metallic powder and mainly consist of Ni and Al, Mo, O, Ti. On the other hand, the darker splats consist of chemical elements such as Ti, Al and O and were made from the Al_2O_3–40%TiO_2 ceramic powder. A morphology analysis indicates that the ceramic lamellas are much more rounded and less flattened than the metallic lamellas.

The manufactured composite coatings have a relatively coarse structure (lamella interfaces are clearly visible), which is typical of LVOF flame sprayed coatings. The examined microstructure exhibits much rounded and large pores compared to the microstructure observed for the coatings prepared by the PS or HVOF methods, as described in [12,14]. This is connected with the impact energy of sprayed particles and process temperature which are different for LOVF than for PS and HVOF processes.

The relationship between porosity and the Al_2O_3–40%TiO_2 feedstock powder composition was studied, **Fig. 4**. Porosity measurements demonstrated that the average porosity of all coatings, except for those with 90%cp and 100%cp, was in the range of 9.8% to 10.8%, while the porosity of coatings with 90%cp and 100%cp was 11.6% and 13.3%, respectively. A denser structure was observed for the 40%cp and 50%cp cermet coatings. In general, the coatings have a relatively high porosity, which is in agreement with the literature of the subject. The porosity of LOVF-sprayed coatings is usually higher than the porosity obtained for PS or HVOF coatings [4,8]. However, relatively high porosity improves fracture toughness and allows the coating to alleviate internal stresses [3], which can have a beneficial effect on their cavitation erosion resistance.

Preprints (www.preprints.org) | NOT PEER-REVIEWED | Posted: 6 June 2018 doi:10.20944/preprints201806.0090.v1

Peer-reviewed version available at Coatings 2018, 8, 254; doi:10.3390/coatings8070254

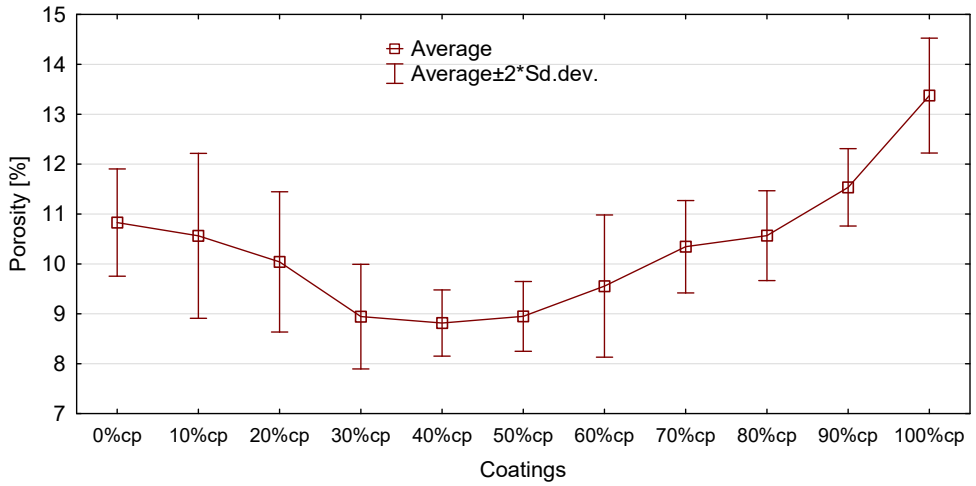

Fig. 4 Influence of the ceramic powder (cp) content on coating porosity

The as-sprayed coating surface roughness is attributed to the presence of lamellar structure, the unmelted particles and the overlapping of splats. The surface roughness Ra of the as-sprayed cermet coatings range from 23.4 μm to 28.2 μm, while the Ra values of the 0%cp metallic bond-coat and the ceramic top coating with 100%cp amount to 17.5 μm and 18.8 μm, respectively. It can be seen in Fig 3 and Fig. 5 that the morphology of the as-sprayed coating develops qualitatively and quantitatively in agreement with the changes of ceramic feedstock powder. The Ra roughness parameter increases until the 50% content of cp in the sprayed powder mixtures (Fig. **5**) and then decreases with increasing the content of cp. Moreover, the Ra value of the as-sprayed coating with a 100%cp feedstock powder Al_2O_3–40%TiO_2 top layer is comparable with the same type of top layer coating presented by Mishra et al. [2], which confirms that the spraying process parameters were correct.

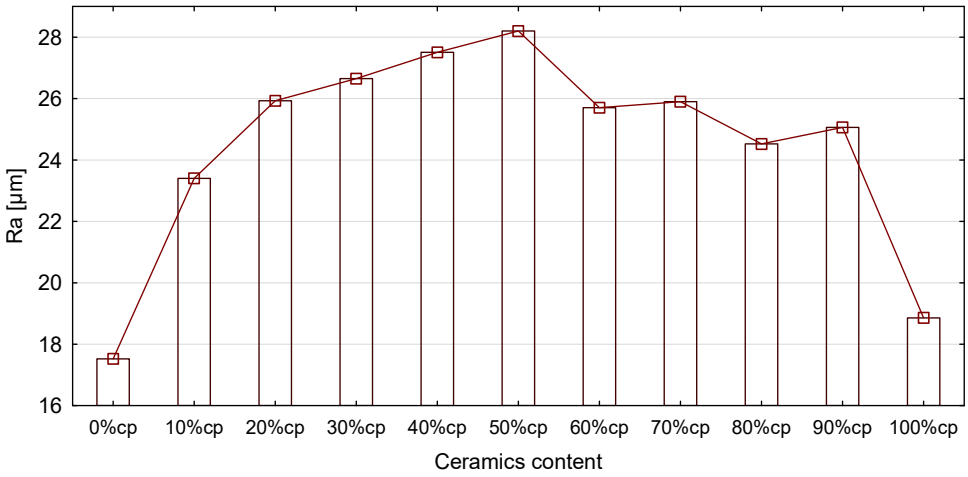

Fig. 5 Effect of the ceramic powder (cp) content on coating surface roughness

The XRD patterns of the bond layer (100%mp), cermet top layer (blend with 50%mp and 50%cp) and ceramic top layer sprayed with cp only are shown in Fig. **6**. An examination of the XRD spectra revealed that the bond coat is composed of nickel solid solution and nickel oxide, while the coating produced with 100%cp consists of the aluminium titanate Al_2TiO_5 phase. The cermet coating with 50% of Al_2O_3–40%TiO_2 is composed of the nickel solid solution and the Al_2TiO_5 phase. In the spectra, phases such as rutile (TiO_2) and Al_2O_3 were not found. TiO_2 melts at lower temperature (1854 °C) than Al_2O_3 (2040 °C) [27], and the presence of solid solution with γ-Al_2O_3 was suggested by Mishra et al. [9]. However, the subsequent decomposition of Al_2TiO_5 into rutile (TiO_2) and Al_2O_3 can occur due to

Preprints (www.preprints.org) | NOT PEER-REVIEWED | Posted: 6 June 2018 doi:10.20944/preprints201806.0090.v1

Peer-reviewed version available at Coatings 2018, 8, 254; doi:10.3390/coatings8070254

high temperature >1280 °C [3]; decomposition can also occur if the coating is subjected to high temperature, e.g. in the diesel engine, as discussed in [16].

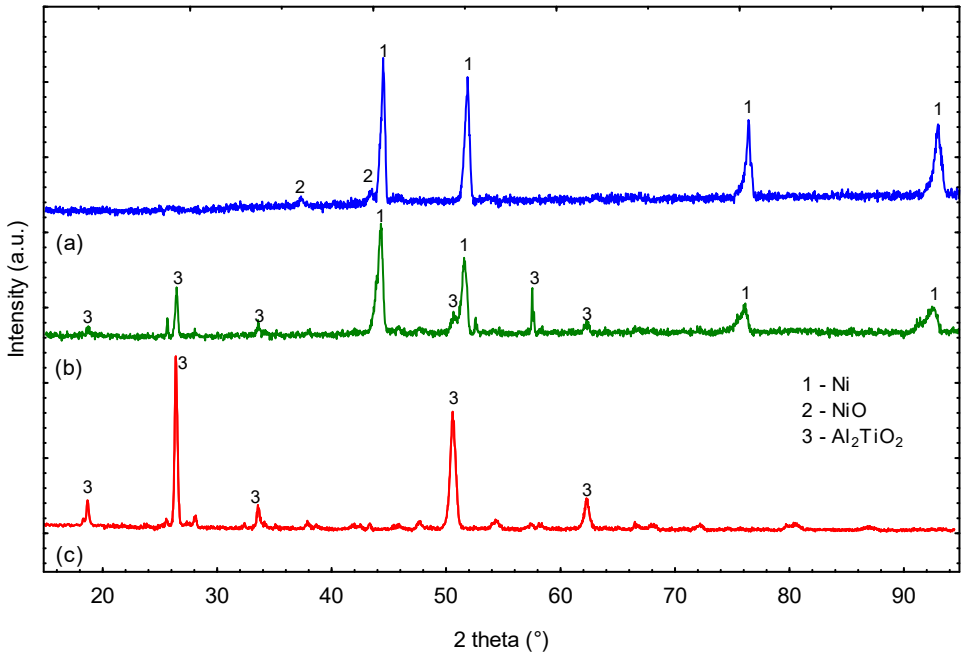

Fig. 6 XRD pattern of as-sprayed (a) – bond layer, (b) coating with 50%cp; (c) – coating sprayed with 100% of ceramic powder

Results of the hardness and Young's modulus examination of the main cermet coating phases are presented in **Tab. 3**. The hardness of the ceramic phase is more than two times higher than that of the metallic phase, in contrast to the Young modulus value that is slightly lower for the ceramic than for metallic phase. The results of hardness and Young's modulus indicate that the ceramic lamellas are more brittle than metallic. The results presented in **Tab. 3** are in line with previous findings of the authors [15]. The hardness is in the range of hardness values presented in [2] for the LVOF-sprayed Al_2O_3–40%TiO_2 coatings, but is lower than that of PTA [10,11] or HVOF [12] Al_2O_3–TiO_2 coatings. The relatively wide range of hardness values demonstrates that the coating microstructure incorporates porosity, voids and defects formed by partially melted or unmelted powder particles, which is in agreement with metallographic results. Also, the hardness value range for the LVOF coatings is clearly wider than that obtained for the PS coatings, which results from a less dense structure of the coatings deposited by the LVOF than those produced by the HVOF or PS processes.

Tab. 3 Mechanical properties of the coatings

Microstructure phase	Nanohardness [HV]		Young's modulus [GPa]	
	Range	Average	Range	Average
Ceramic lamellas	419.1-1286.4	723.2	84.7-141.6	110.4
Metallic lamellas	279.2-386.9	325.5	92.2-187.3	116.8

The results demonstrate that the deposited coatings have a uniform structure and desired technological properties, and hence they can be subjected to cavitation erosion testing.

3.2 Cavitation erosion

Results of the cavitation erosion investigation are presented in **Fig. 7**-**Fig. 15**. The ultrasonic test stand used in our research generates intensive cavitation in comparison to other types of testing equipment [23]. Thus, the effect of the cavitation wear of sprayed coatings was determined in a relatively short period of time, in contrast to that observed for the reference bulk alloys. In the

Preprints (www.preprints.org) | NOT PEER-REVIEWED | Posted: 6 June 2018 doi:10.20944/preprints201806.0090.v1

Peer-reviewed version available at Coatings 2018, 8, 254; doi:10.3390/coatings8070254

cavitation erosion process, the acceleration and deceleration stages of erosion can be distinguished, usually incubation. These stages occur especially during the testing of metal alloy samples according to ASTM G-32, and the incubation stage can easily be distinguished [25,28,29]. On the other hand, the wear of ceramic materials differs from that observed for metal alloys. The initial stage of cavitation erosion of ceramic samples can be very short, as reported for alumina in [30].

An analysis of the cavitation erosion curves (**Fig. 7**) of the tested sprayed Al_2O_3–40%TiO_2/NiMoAl coatings reveals that the incubation stage is negligible. In addition, the mass loss rate is constant for every tested cermet coating, otherwise than for the metal alloy (AlSi). Jafarzadeh and Ghavidel [10] observed a similar effect for the plasma-sprayed Al_2O_3–13%TiO_2 coatings, however they did not tested any reference material, therefore a comparison of the results is difficult. In our study, the cermet coatings and metal alloys (structural steel FeC, brass CuZn and cast aluminium alloy AlSi) were tested in similar test condition. Apart from the AlSi sample, the FeC and CuZn metal alloy samples showed negligible mass loss after the test time. The surfaces of cavitation-worn reference samples are shown in **Fig. 8**.

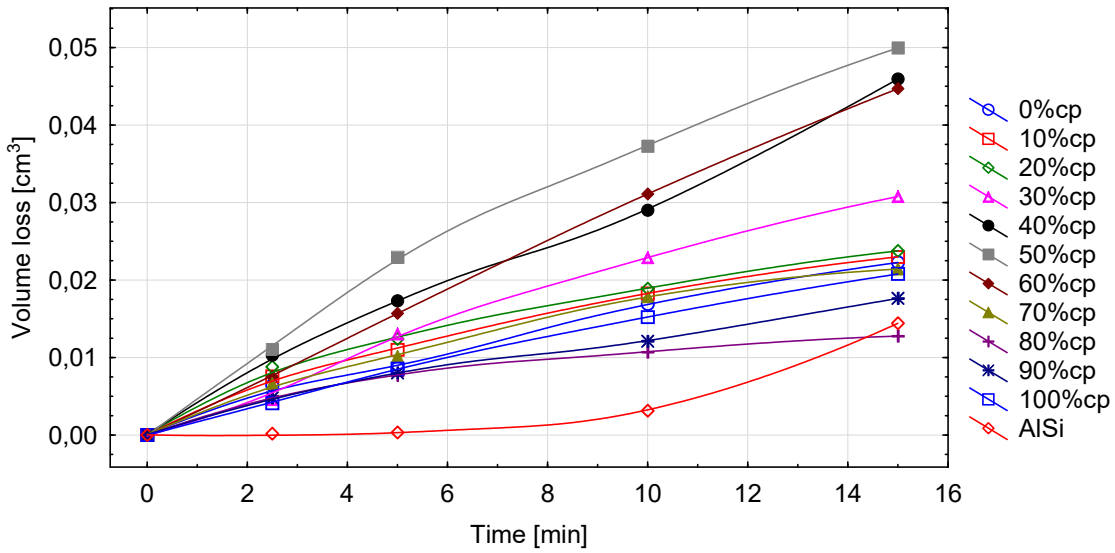

Fig. 7 Cumulative erosion-time curves for the tested coatings

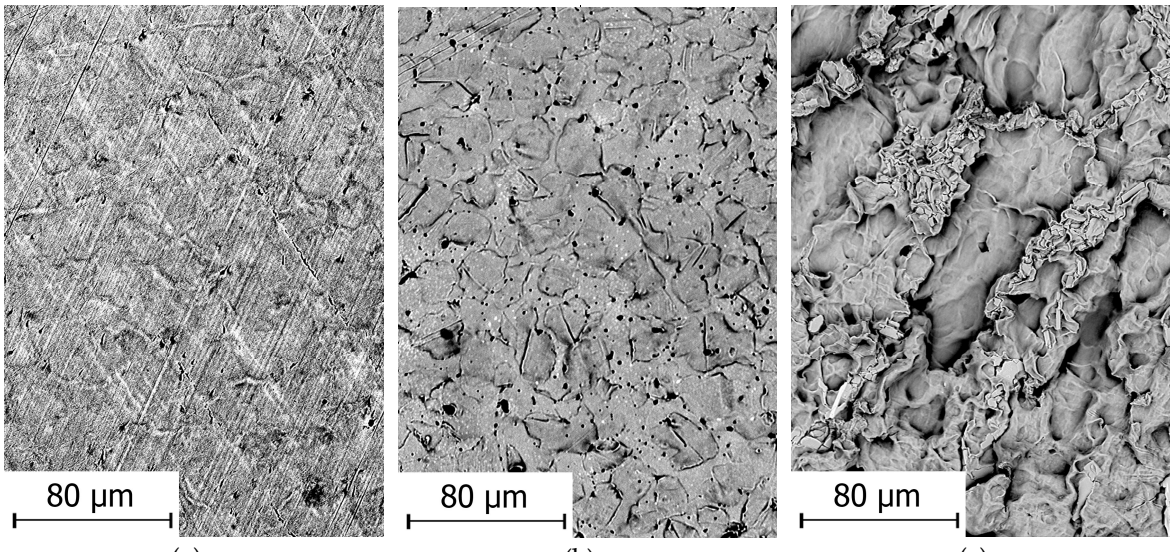

Fig. 8 Cavitation-worn surface of metal samples: a - FeC (15 min), b - CuZn (15 min), c - AlSi (5 min), SEM

Cavitation erosion is a fatigue process. After cavitation erosion incubation period, specific for each metal alloy, occurs material loss and pits start to develop on its surface. The wear of metal alloys

Preprints (www.preprints.org) | NOT PEER-REVIEWED | Posted: 6 June 2018 doi:10.20944/preprints201806.0090.v1

Peer-reviewed version available at Coatings 2018, 8, 254; doi:10.3390/coatings8070254

usually starts from plastic deformation of metal grains due to the impact of hydrodynamic cavitation. After 15 minutes of cavitation, the FeC samples (**Fig. 8**a) show changes in their surface topography; also, the surface of the CuZn sample (**Fig. 8**b) is deformed and some pits are visible, however the mass loss is within the range of measurment error. On the other hand, AlSi exhibits a heavily eroded surface (**Fig. 8**c) and material loss (**Fig. 7**). An analysis of the cavitation erosion curves and damaged surfaces of the reference samples (**Fig. 7** and **Fig. 8**) allows us to state that the tested aluminium alloy exhibits an accelerated stage of erosion, while the FeC and CuZn samples show an incubation period of cavitation. The wear mechanism of AlSi was discussed in detail in our previous work [29]. It is known that the fine grain structure of wrought metal alloys has a beneficial impact on their resistance to cavitation erosion. Therefore, AlSi has a typical as-cast coarse dendritic structure, which accelerates cavitation erosion. AlSi is less resistant to cavitation erosion than FeC and CuZn specimens. Thus, the normalised erosion resistance of coatings was calculated in relation to the AlSi sample, presented in **Fig. 9**. The cermet Al_2O_3–40%TiO_2/NiMoAl coating exhibits a relatively low resistance to cavitation. The lowest resistance to cavitation was identified for the coating with 50% of cp, for which the normalized erosion resistance equals 0.22, which is four times lower than the highest cavitation resistance observed for the coating containing 80%cp. Therefore, the coatings sprayed with 80% of Al_2O_3–40%TiO_2 feedstock powder seem optimal for cavitation erosion resistance of the tested cermet coatings, **Fig. 9**, **Fig. 10**. The mass content of Al_2O_3–40%TiO_2 in Al_2O_3–40%TiO_2 /NiAlMo mixture feedstock powders influences the cermet roughness and porosity, and – in effect – its cavitation erosion resistance, **Fig. 11** and **Fig. 12**.

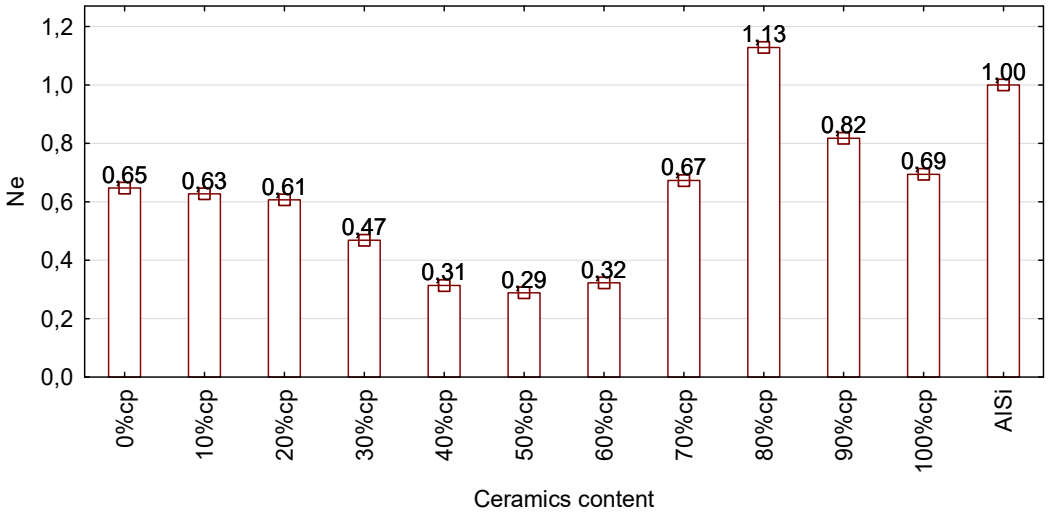

Fig. 9 Normalized cavitation erosion resistance of the coatings

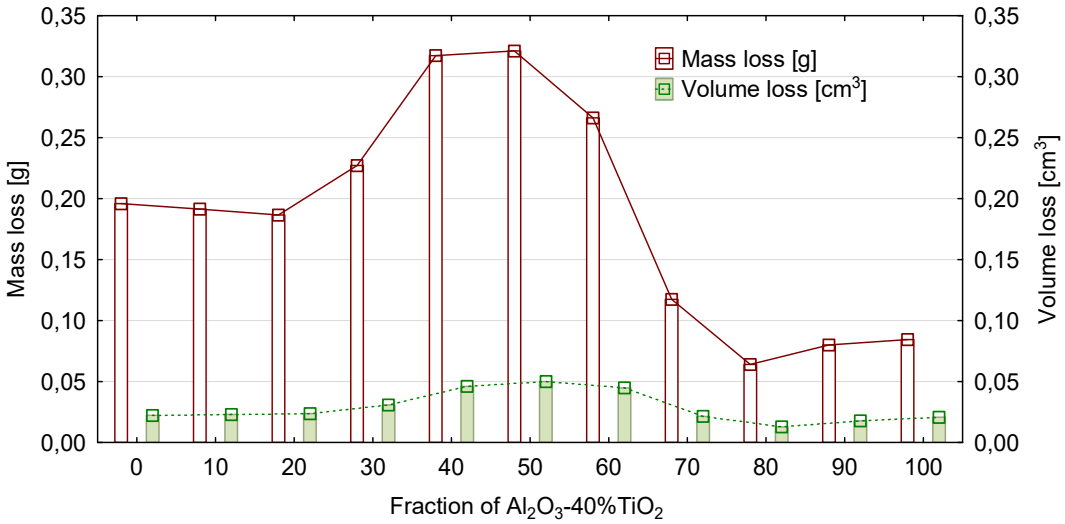

Preprints (www.preprints.org) | NOT PEER-REVIEWED | Posted: 6 June 2018 doi:10.20944/preprints201806.0090.v1

Peer-reviewed version available at Coatings 2018, 8, 254; doi:10.3390/coatings8070254

Fig. 10 Influence of the Al_2O_3–40%TiO_2 content on coating material loss

Although no strong correlation was found, we claim that the coating roughness and porosity affect its cavitation erosion resistance, **Fig. 11** and **Fig. 12**. Generally, with increasing the cermet coating roughness we can observe a decrease in the cavitation erosion resistance (**Fig. 11**). On the other hand, the increase in porosity has a positive effect on improving the coating cavitation erosion resistance, **Fig. 12.** Moreover, this agrees with Cui et al. [3], who observed that the high coating porosity improves fracture toughness and alleviates the coating internal stresses [3]. These phenomena can have a positive effect on the cavitation erosion resistance of cermet coatings.

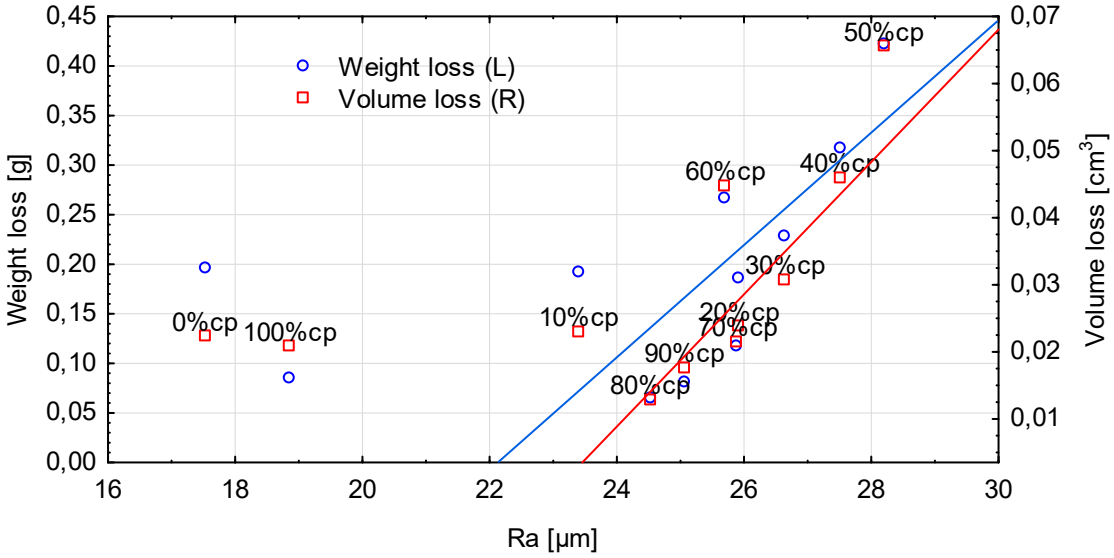

Fig. 11 Influence of the coating roughness on its mass and volume loss, 15 minutes of the cavitation test

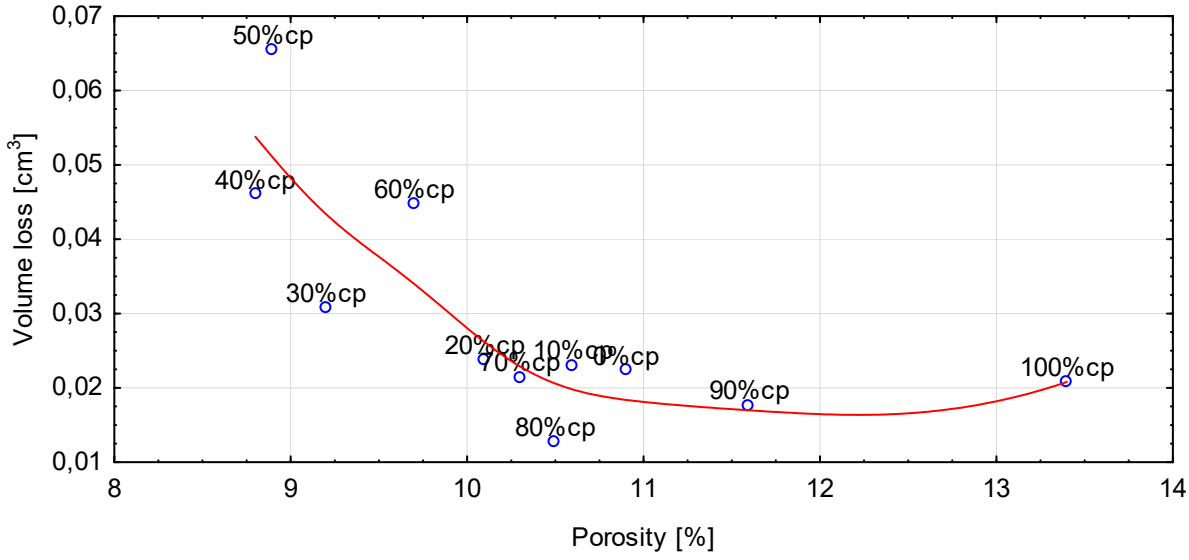

Fig. 12 Effect of the coating porosity on cumulative volume loss

3.3. Cavitaiton erosion mechanism and the phenomenological model of Al_2O_3–40%TiO_2/NiMoAl coatings

The cavitation erosion mechanism of Al_2O_3–40%TiO_2/NiMoAl coatings is investigated based on systematic SEM-EDS and LOM observations, the results of investigations are shown in **Fig. 13**-**Fig. 15**. Moreover, the progression of cermet coating erosion was analysed by comparing the as-sprayed coatings (shown in **Fig 3**) with those subjected to cavitation tests, **Fig. 13** and **Fig. 14**. The progression of cermet coating cavitation erosion was analysed based on observations conducted at different time

Preprints (www.preprints.org) | NOT PEER-REVIEWED | Posted: 6 June 2018 doi:10.20944/preprints201806.0090.v1

Peer-reviewed version available at Coatings 2018, 8, 254; doi:10.3390/coatings8070254

intervals (**Fig. 15**). In effect, a general phenomenological model of Al_2O_3–40%TiO_2/NiMoAl cermet cavitation erosion was elaborated, see **Fig. 16**.

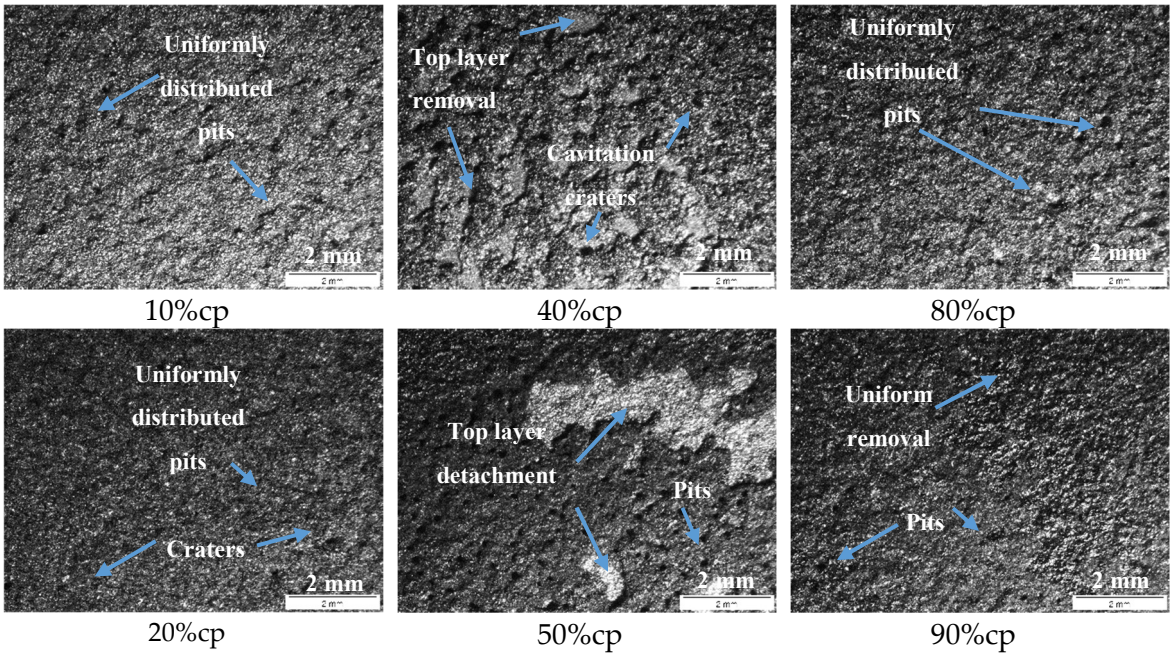

Fig. 13 Cavitation-worn surfaces of Al_2O_3–40%TiO_2/NiMoAl cermet coatings deposited with various ceramic powder contents %cp, LOM – stereoscope microscope

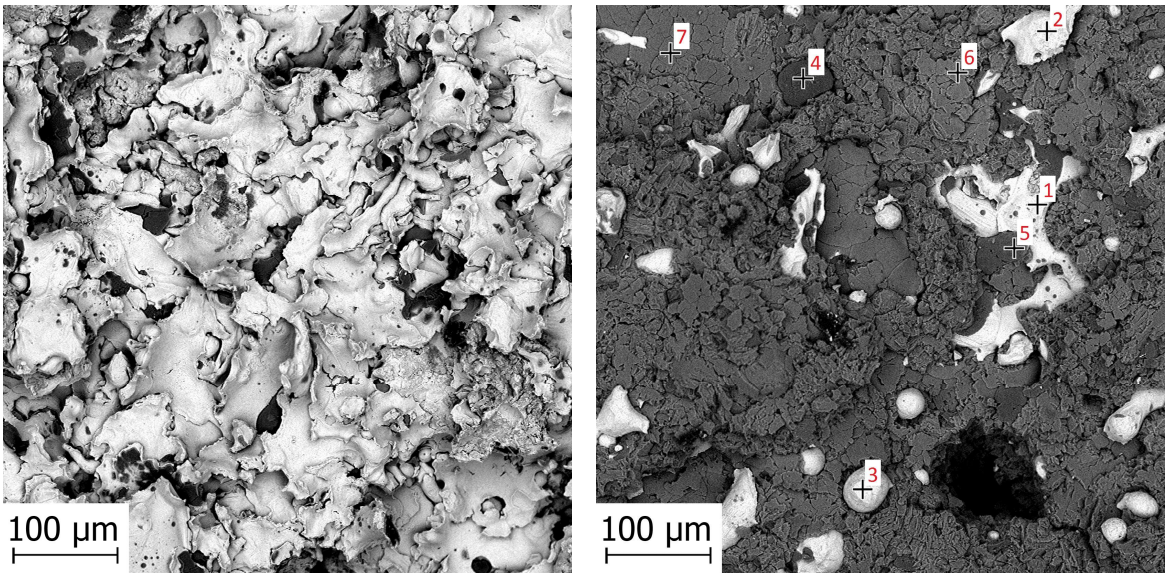

Preprints (www.preprints.org) | NOT PEER-REVIEWED | Posted: 6 June 2018 doi:10.20944/preprints201806.0090.v1

Peer-reviewed version available at Coatings 2018, 8, 254; doi:10.3390/coatings8070254

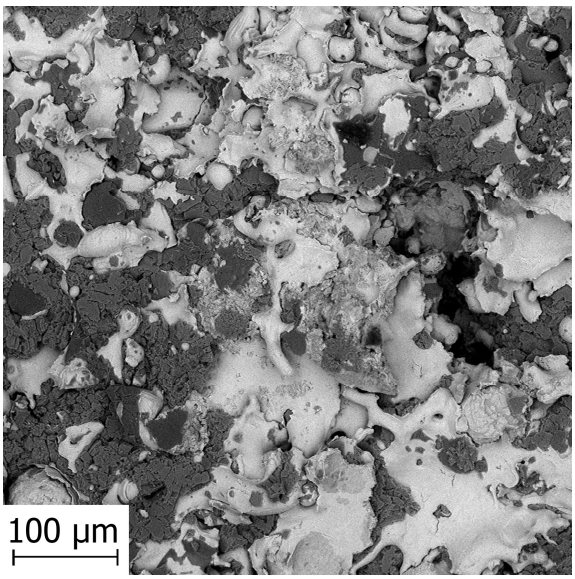

30%cp

Element concentration [wt.%], see Fig. 80%cp					
	Ni	Mo	Al	Ti	O
1	67.4±2.4	5.1±6.1	9.6±3.5	3.9±5.7	14.1±4.3
2	60.2±2.2	3.5±8.4	11.7±3.0	5.1±4.8	19.4±3.6
3	64.8±2.0	4.3±7.7	7.9±4.0	3.4±6.5	19.6±3.6
4			38.3±0.9	3.4±4.7	58.3±1.4
5			48.6±1.2	5.6±5.1	45.8±2.6
6			22.2±1.7	51.1±2.8	26.7±2.0
7			25.8±1.6	47.6±3.0	26.6±2.0

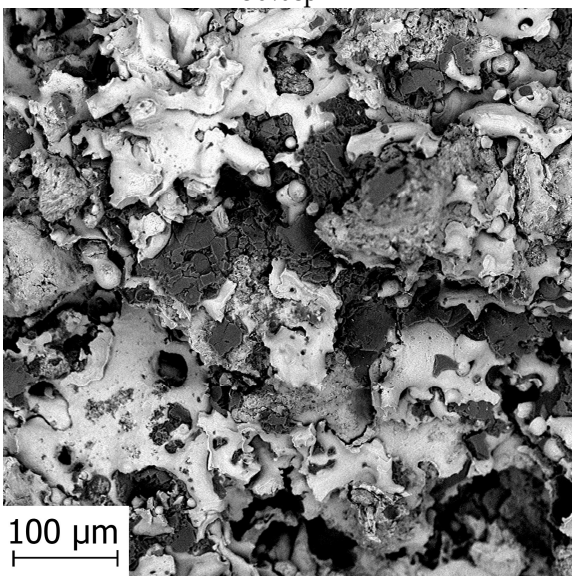

60%cp

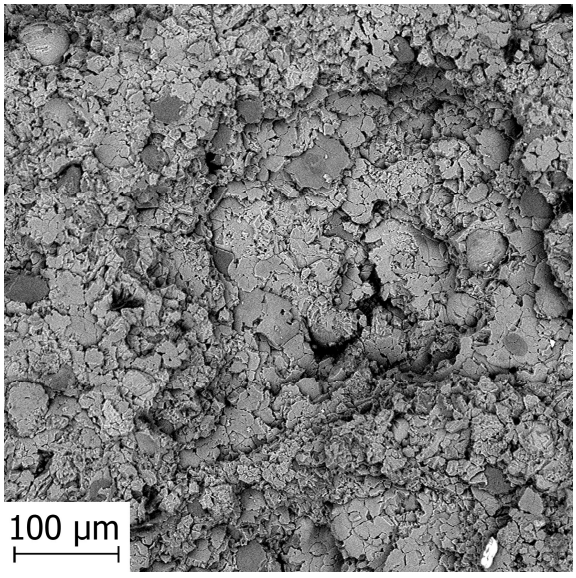

100%cp

Fig. 14 Coatings after 15 minutes of the cavitation test, SEM and results of 80%cp spot chemical analysis, SEM-EDS. Worn surfaces of the coatings correspond to the as-sprayed surfaces shown in Fig 3.

The effect of cp content on the erosion of coatings was studied on the basis of macroscopic (**Fig. 13**) and microscopic (**Fig. 14**) observations. The erosion of cermet Al_2O_3–40%TiO_2/NiMoAl coatings deposited with 10-30%cp and 70-90%cp proceeds at almost constant rate with a uniform pit distribution, whereas the erosion of coatings produced with 40-60%cp consists in the removal of massive chunks of material and the formation of craters, as shown in **Fig. 13**. After 15 min of test time, huge pits in the coating were recognized and the bond coat was exposed, **Fig. 13** and **Fig. 14**. The CER of the samples produced with the highest contents of powders is at the similar level, as confirmed by the plot in **Fig. 10**. The mass decrement in the coatings mainly composed of metallic feedstock powder with the addition of 10% to 30 cp is similar, **Fig. 10**. Similar results can be observed for the coatings sprayed with a high content of ceramic with 80% to 100% of cp. In general, the cavitation wear of coatings with higher titania-alumina contents exhibits a more uniform pattern than the erosion of coatings enriched with the metallic phase, **Fig. 13** and **Fig. 14**. This results from a combination of cermet properties, uniform morphology and lower surface roughness (**Fig. 5**) of the cermet coating with a higher titania-alumina content than the metallic phase. It seems that the differences between the metallic and ceramic lamella properties such as hardness and Young's

modulus, (**Tab. 3**) affect the cavitation erosion process of cermet Al_2O_3–40%TiO_2/NiMoAl. Conducted investigations reveal that the hard and brittle Al_2O_3–TiO_2 phase is more susceptible to cavitation erosion than NiMoAl splats, and so the cermet erosion starts in ceramic lamellas, **Fig. 14**. Also, it is known from the literature that surface uniformity has a positive effect on the CER. The cermet composition ratio of ceramic and metallic powders affects the resistance to cavitation wear. Thus, the addition of 20% of NiMoAl feedstock powder prevents the ceramic phases from detachment in massive chunks. Summing up, we maintain that 80% portion of Al_2O_3–40%TiO_2 in Al_2O_3–40%TiO_2/NiMoAl mixture is optimal for the cavitation erosion resistance of cermet coatings.

Observations conducted at higher magnification (**Fig. 15**) allow to formulate the general mechanism of cavitation erosion of Al_2O_3–40%TiO_2/NiMoAl. The heterogeneous structure of the LVOF thermally-sprayed coatings consists of ceramic and metallic lamellas, partially or unmelted particles, lamella interfaces, porosity and microcracks. It was demonstrated by the LOM, SEM and EDS chemical analysis (**Fig 2**, **Fig 3** and **Fig. 14**) that two main lamellas in cermet structure are metallic (NiMoAl) and ceramic (Al_2O_3–40%TiO_2). A model of the cermet structure is presented in **Fig. 16**a, and the mechanism of cavitation erosion is schematically described in **Fig. 16**b-c.

The process of material removal from cermet coatings starts almost without the incubation period of cavitation erosion, see the plot in **Fig. 7**. The first stadium of erosion was the removal of splats with low coherence, then the edges of overlapping particles or loose splats were detached (compare **Fig 3** and **Fig. 14**). As mentioned before, coating morphology and roughness affect the cavitation erosion of cermet. The degradation of cermet structure mainly depends on the removal of ceramic Al_2O_3–TiO_2 lamellas, as shown in **Fig. 16**b. It is demonstrated in **Fig. 15**a, b that the structure inhomogeneity such as the formation of primary microcracks in ceramic lamellas plays a major role in the initiation of erosion, resulting in ceramic crushing and spalling. Ceramic splats have higher brittleness (**Tab. 3**) than metallic ones, so the identified cavitation erosion mechanism was brittle fracture, **Fig. 15**c. These microcracks propagate though the ceramic lamellas and get connected with voids, pits and other cracks, consequently eliminating the ceramic phase from the cermet structure. The coating microstructure exhibits porosity, which also influences the cavitation wear of cermet (**Fig. 4**). The erosion propagates toward the ceramic lamellas, **Fig. 15**d, and continues by the removal of exposed metallic splats and unmelted particles, see **Fig. 14** and **Fig. 15**a,b,e,g. Exposed to cavitation damage, metallic lamellas undergo cracking, as shown in **Fig. 15**f,g,h. In particular, the edges of overlapping metallic splat lamellas undergo cavitation erosion and the whole unmelted particles are taken out (**Fig. 16**c and **Fig. 15**d,e). Then, the alternating removal of cermet structural components proceeds in the bond layer direction. Once the cracks connect with the pores, deep cavitation pits (craters) can occur, **Fig. 15**i, j and **Fig. 16**c. Then, metallic lamellas lose support form ceramic and depart from the cermet. This results in the cracking and extraction of metallic lamellas, which consequently leads to metallic splat detachment, as shown in **Fig. 16**d and made visible in **Fig. 15**f. The erosion process proceeds alternatively splat-by-splat, towards the bond layer, **Fig. 15**g, h. Finally, the developed severe erosion progresses even through the whole cermet coating, so large craters are formed (**Fig. 13**), as described in **Fig. 16**d. The cavitation erosion of cermet coatings progresses, resulting in the worn-surface roughening, which accelerates the decrement of coating material in form of large blocky particles or the detachment of whole splats, as shown in **Fig. 13**.

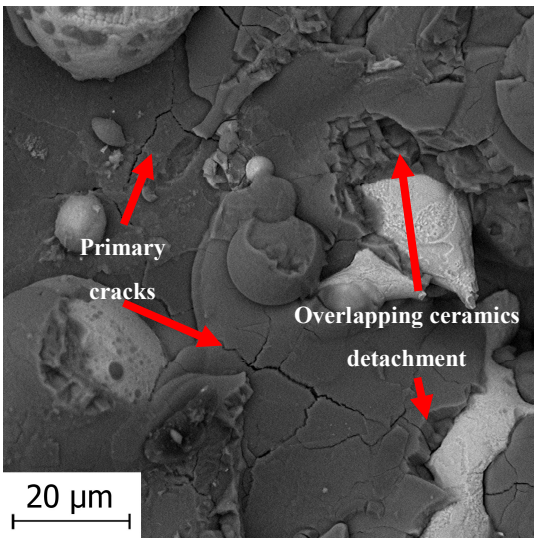

(a) Initial cracks and removal of ceramics top of metallic splats, 80%cp, 5 min

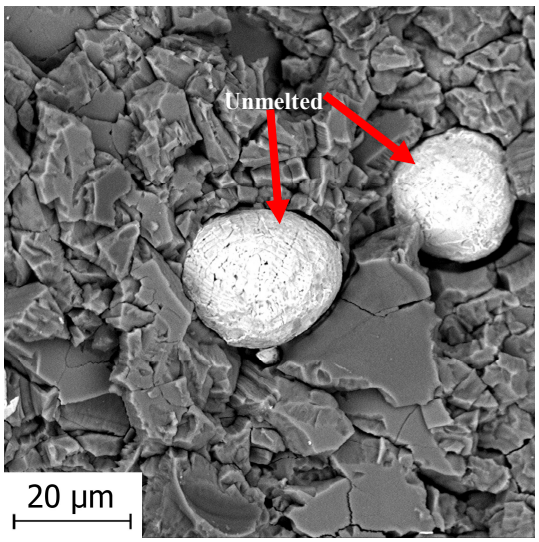

(b) Fragmentation of ceramics and the exposition of unmelted metallic particles, 80%cp, 10 min

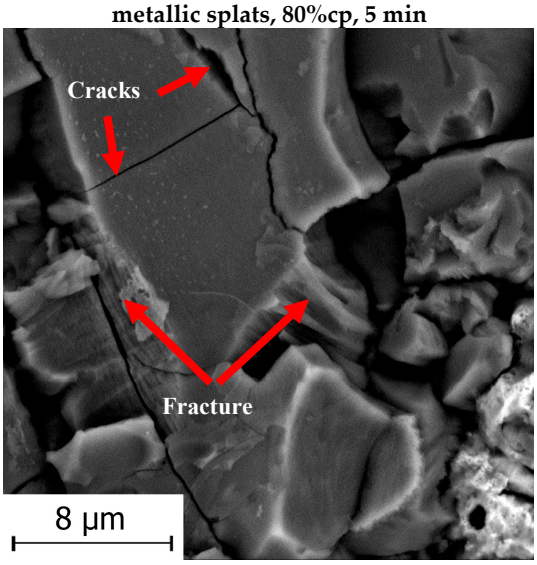

c) Brittle fracture and cracks in ceramic lamellas, 60%cp, 5 min

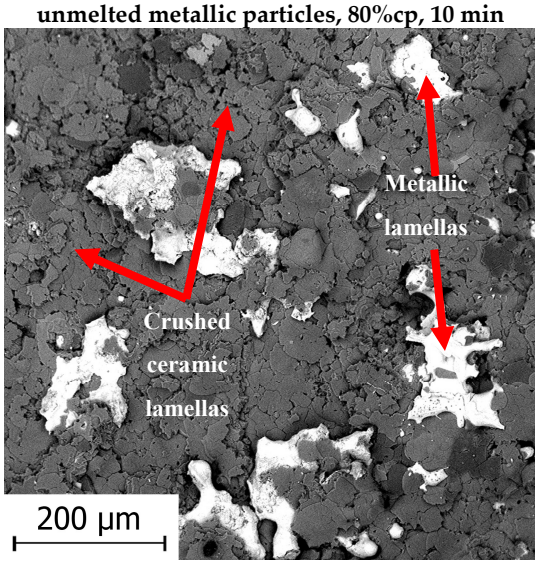

d) Exposition of metallic splats due to ceramic removal, 90%cp, 10 min

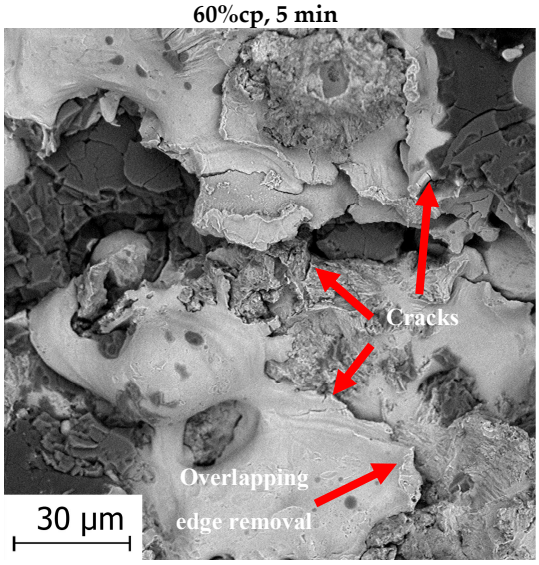

e) Detachment of overlapping metallic lamellas starting at the edges, 20%cp, 5 min

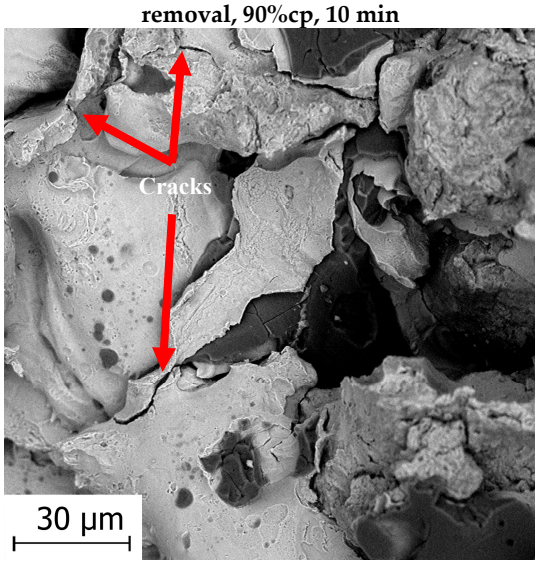

f) Formation of cracks in the exposed metallic phase, 40%cp, 10 min

Preprints (www.preprints.org) | NOT PEER-REVIEWED | Posted: 6 June 2018 doi:10.20944/preprints201806.0090.v1

Peer-reviewed version available at Coatings 2018, 8, 254; doi:10.3390/coatings8070254

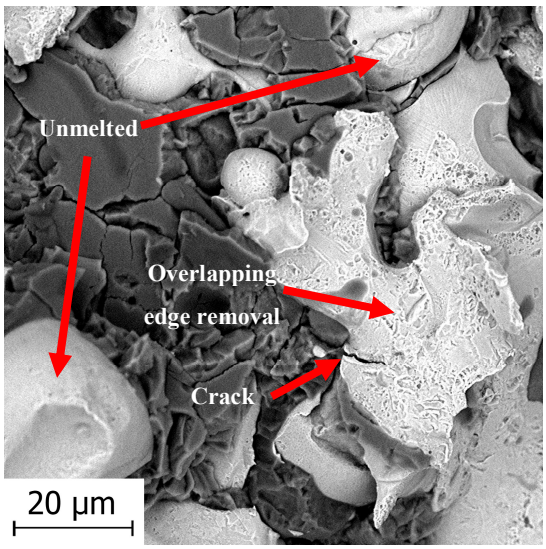

(g) Removal of phases starting with the removal of ceramic, metallic splat edges, exposition of unmelted particles, 50%cp, 5 min

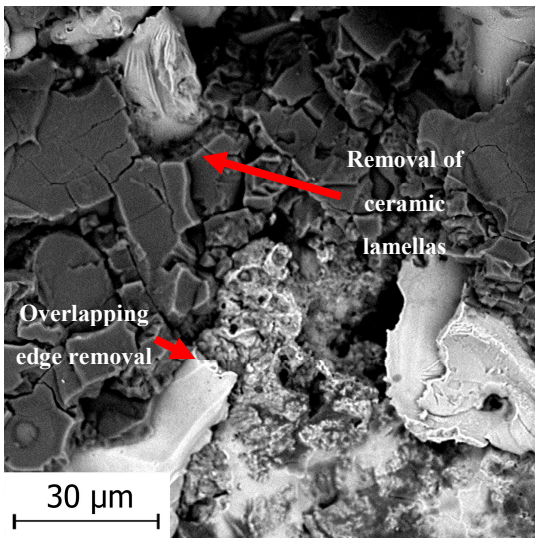

(h) Alternate removal of splats starting with the detachment of ceramic lamellas and metallic splat edges, 60%cp, 10 min

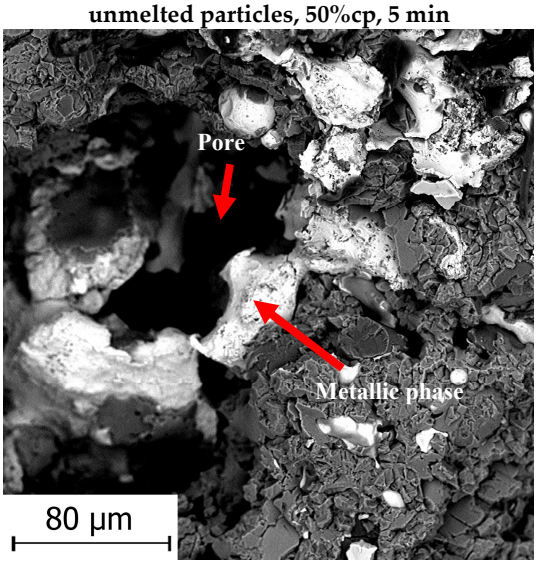

i) Pit growth due coating material removal and connection with inhomogeneity (pore), 50%cp, 10 min

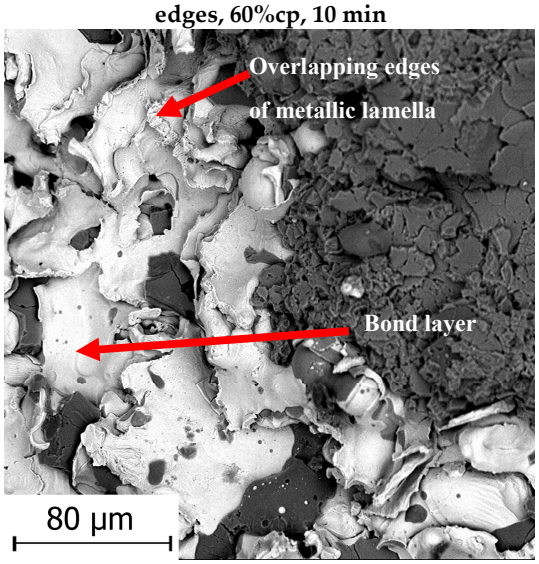

j) Edge of the crater, bond layer exposed. Detachment of the overlapping metallic lamella, 70%cp, 15 min

Fig. 15 Selected areas of cavitation-worn cermet coatings observed at different time intervals, SEM

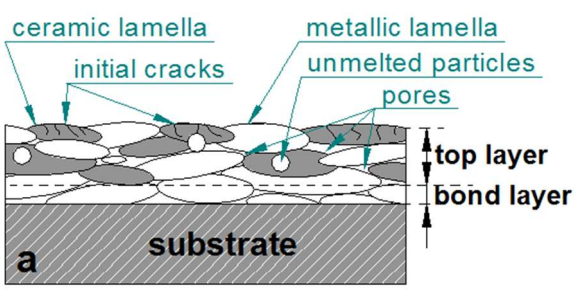

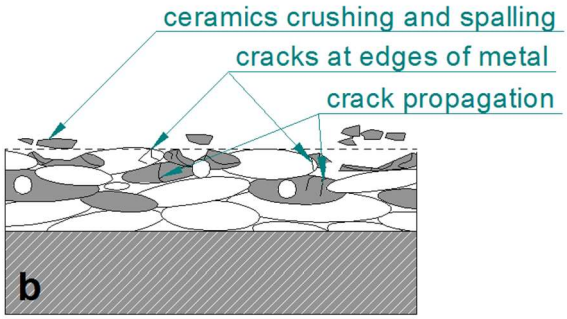

Preprints (www.preprints.org) | NOT PEER-REVIEWED | Posted: 6 June 2018 doi:10.20944/preprints201806.0090.v1

Peer-reviewed version available at Coatings 2018, 8, 254; doi:10.3390/coatings8070254

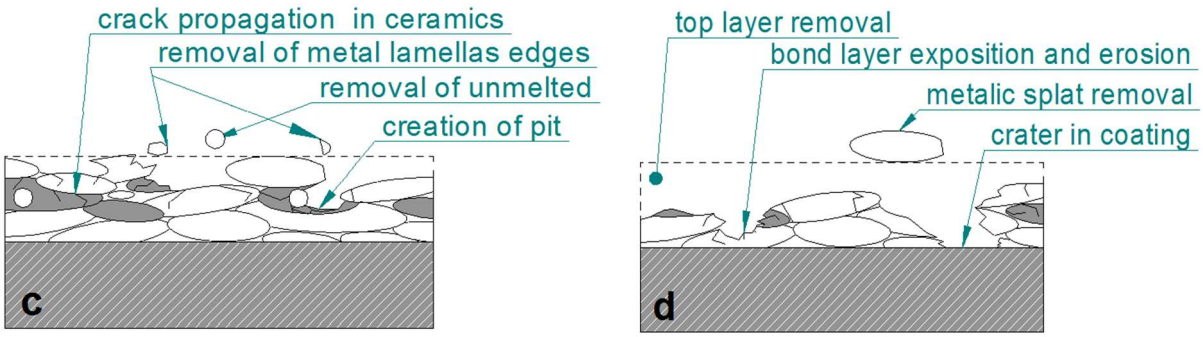

Fig. 16 Phenomenological model of cermet coating cavitation erosion: (a) - coating before cavitation, (b-d) successive changes in the coating due to cavitation erosion

4. Conclusions

In this study, the cavitation wear test of the Al_2O_3–40%TiO_2/NiMoAl cermet coatings deposited by LVOF onto steel substrates was performed. The cavitation erosion resistance and wear mechanism of the flame-sprayed Al_2O_3–40%TiO_2/NiMoAl cermet coatings as well as the effect of feedstock powder ratios (Al_2O_3–TiO_2/NiMoAl) of deposited cermet coatings on their cavitation erosion resistance was determined. General relationships between the properties, microstructure and cavitation wear resistance of the coatings were examined and the following conclusions were drawn:

- Cermet coatings sprayed with the mixtures of Al_2O_3–40%TiO_2 and NiMoAl feedstock powders were successfully deposited by LVOF. The lamellar structure of sprayed cermet incorporating unmelted particles, ceramic and metallic lamellas, lamella interfaces, porosity, oxide particles and microcracks was identified. The average hardness of ceramic and metallic lamellas is 727 HV and 327 HV, respectively. The porosity was in the range of 9.8-13.3%. The surface roughness Ra of as-sprayed cermet ranged from 23.4 μm to 28.2 μm.
- The composition of a blend of the Al_2O_3–40%TiO_2 and NiAlMo mixture of feedstock powders affects the cavitation erosion resistance of cermet coatings. The coating sprayed with the mixture containing 80 wt% of Al_2O_3–40%TiO_2 exhibits a higher cavitation erosion resistance than other cermet. Thus, the addition of 20% of metal is optimal for cavitation erosion resistance of the Al_2O_3–40%TiO_2/NiMoAl cermet.
- The cermet coating sprayed with the Al_2O_3–40%TiO_2/NiAlMo mixture containing 80 wt% of Al_2O_3–40%TiO_2 has more than 10% higher normalised cavitation erosion resistance than the reference aluminium alloy. However, the cavitation wear rates of the cermet coatings were higher than those of the reference steel and brass samples.
- The difference in cavitation erosion of the coatings and metal alloys depends on the constant erosion rate identified for the coatings. Contrary to the reference aluminium alloy, the incubation stage of cavitation erosion is negligible in the case of the cermet coatings.
- On the whole, porosity and surface roughness affect cavitation erosion resistance (CER). Increased porosity or/and decreased surface roughness have a positive effect on the CER of cermet coatings.
- The investigation revealed that the hard and brittle ceramic phase is more susceptible to cavitation erosion than metallic splats. A dominant mechanism of the cavitation erosion of composite coatings is brittle fracture initiated by the formation of primary microcracks in ceramic lamellas and followed by ceramic phase removal. Then, exposed to cavitation, the metallic lamellas undergo erosion consisting in the removal of overlapping edges or/and whole metallic splats.
- A general cavitation erosion phenomenological model of the Al_2O_3–40%TiO_2/NiMoAl cermet coatings was elaborated. The model relies on the erosion of cermet lamellas initiated by the removal of ceramic lamellas. The mechanism of cavitation erosion is accelerated by cermet

structural nonuniformities or discontinuities such as the primary crack network, unmelted particles and porosity, and depends on the differences in the mechanical properties of ceramic and metallic lamellas. The study confirmed that any inhomogeneity such as primary microcracks in ceramic lamellas play a major role in the initiation of erosion, which leads to ceramic crushing and spalling.

Acknowledgments: The research was financed under the grant no. S2/M/2018 of the Lublin University of Technology, Poland.

Author Contributions: M. Szala and T. Hejwowski conceived and designed the experiments; T. Hejwowski sprayed the coatings. M. Szala performed the cavitation erosion tests; M. Szala and T. Hejwowski analyzed the data; M. Szala wrote the paper; T. Hejwowski revised the manuscript.

Conflicts of Interest: The authors declare no conflict of interest.

References

1. Gao, X.; Tian, Z.; Liu, Z.; Shen, L. Interface characteristics of Al2O3-13%TiO2 ceramic coatings prepared by laser cladding. *Trans. Nonferrous Met. Soc. China* **2012**, *22*, 2498–2503, doi:10.1016/S1003-6326(11)61491-X.
2. Mishra, N. K.; Mishra, S. B. Hot corrosion performance of LVOF sprayed Al2O3–40% TiO2 coating on Superni 601 and Superco 605 superalloys at 800 and 900°C. *Bull. Mater. Sci.* **2015**, *38*, 1679–1685, doi:10.1007/s12034-015-0986-9.
3. Cui, S.; Miao, Q.; Liang, W.; Zhang, Z.; Xu, Y.; Ren, B. Tribological Behavior of Plasma-Sprayed Al2O3-20 wt.%TiO2 Coating. *J. Mater. Eng. Perform.* **2017**, *26*, 2086–2094, doi:10.1007/s11665-017-2653-3.
4. Davis, J. R. *Handbook of Thermal Spray Technology*; ASM International, 2004; ISBN 978-0-87170-795-6.
5. Czupryński, A. Selected Properties Of Thermally Sprayed Oxide Ceramic Coatings. *Adv. Mater. Sci.* **2015**, *15*, 17–32, doi:10.1515/adms-2015-0012.
6. Szymański, K.; Hernas, A.; Moskal, G.; Myalska, H. Thermally sprayed coatings resistant to erosion and corrosion for power plant boilers - A review. *Surf. Coat. Technol.* **2015**, *268*, 153–164, doi:10.1016/j.surfcoat.2014.10.046.
7. Yao, Y.; Lyckfeldt, O.; Tricoire, A.; Tricoire, A. Microstructure of Plasma Sprayed Al2O3-3wt%TiO2 Coating Using Freeze Granulated Powder. *J. Mater. Sci. Chem. Eng.* **2016**, *04*, 8, doi:10.4236/msce.2016.47002.
8. Jia, S.; Zou, Y.; Xu, J.; Wang, J.; Yu, L. Effect of TiO2 content on properties of Al2O3 thermal barrier coatings by plasma spraying. *Trans. Nonferrous Met. Soc. China* **2015**, *25*, 175–183, doi:10.1016/S1003-6326(15)63593-2.
9. Mishra, N. K.; Mishra, S. B.; Kumar, R. Oxidation resistance of low-velocity oxy fuel-sprayed Al2O3-13TiO2 coating on nickel-based superalloys at 800°C. *Surf. Coat. Technol.* **2014**, *260*, 23–27, doi:10.1016/j.surfcoat.2014.07.089.
10. Jafarzadeh, K.; Valefi, Z.; Ghavidel, B. The effect of plasma spray parameters on the cavitation erosion of Al2O3–TiO2 coatings. *Surf. Coat. Technol.* **2010**, *205*, 1850–1855, doi:10.1016/j.surfcoat.2010.08.044.
11. Morks, M. F.; Akimoto, K. The role of nozzle diameter on the microstructure and abrasion wear resistance of plasma sprayed composite coatings. *J. Manuf. Process.* **2008**, *10*, 1–5, doi:10.1016/j.jmapro.2008.10.001.

12. Matikainen, V.; Niemi, K.; Koivuluoto, H.; Vuoristo, P. Abrasion, Erosion and Cavitation Erosion Wear Properties of Thermally Sprayed Alumina Based Coatings. *Coatings* **2014**, *4*, 18–36, doi:10.3390/coatings4010018.
13. Żórawski, W.; Góral, A.; Bokuvka, O.; Lityńska-Dobrzyńska, L.; Berent, K. Microstructure and tribological properties of nanostructured and conventional plasma sprayed alumina–titania coatings. *Surf. Coat. Technol.* **2015**, *268*, 190–197, doi:10.1016/j.surfcoat.2014.09.014.
14. Maruszczyk, A.; Dudek, A.; Szala, M. Research into Morphology and Properties of TiO2 – NiAl Atmospheric Plasma Sprayed Coating. *Adv. Sci. Technol. Res. J.* **2017**, *11*, 204–210, doi:10.12913/22998624/76450.
15. Hejwowski, T.; Łabacz-Kęcik, A. Mikrostruktura i odporność na zużycie powłok natryskiwanych metodą płomieniowo-proszkową mieszaninami proszków. *Przegląd Spaw. - Weld. Technol. Rev.* **2012**, *9*, 57–64.
16. Hejwowski, T. Comparative study of thermal barrier coatings for internal combustion engine. *Vacuum* **2010**, *85*, 610–616, doi:10.1016/j.vacuum.2010.08.020.
17. Chen, J.; Zhou, H.; Zhao, X.; Chen, J.; An, Y.; Yan, F. Microstructural Characterization and Tribological Behavior of HVOF Sprayed NiMoAl Coating from 20 to 800 °C. *J. Therm. Spray Technol.* **2015**, *24*, 348–356, doi:10.1007/s11666-014-0142-x.
18. Hou, G.; Zhao, X.; Zhou, H.; Lu, J.; An, Y.; Chen, J.; Yang, J. Cavitation erosion of several oxy-fuel sprayed coatings tested in deionized water and artificial seawater. *Wear* **2014**, *311*, 81–92, doi:10.1016/j.wear.2013.12.026.
19. Santa, J. F.; Espitia, L. A.; Blanco, J. A.; Romo, S. A.; Toro, A. Slurry and cavitation erosion resistance of thermal spray coatings. *Wear* **2009**, *267*, 160–167, doi:10.1016/j.wear.2009.01.018.
20. Ksiazek, M.; Boron, L.; Radecka, M.; Richert, M.; Tchorz, A. Mechanical and Tribological Properties of HVOF-Sprayed (Cr3C2-NiCr+Ni) Composite Coating on Ductile Cast Iron. *J. Mater. Eng. Perform.* **2016**, *25*, 3185–3193, doi:10.1007/s11665-016-2226-x.
21. Kekes, D.; Psyllaki, P.; Vardavoulias, M.; Vekinis, G. Wear micro-mechanisms of composite WC-Co/Cr-NiCrFeBSiC coatings.Part II: Cavitation erosion. *Tribol. Ind.* **2014**, *36*, 375–383.
22. Hejwowski, T. Wear resistance of graded coatings. *Vacuum* **2002**, *65*, 515–520, doi:10.1016/S0042-207X(01)00465-1.
23. Steller, J. International Cavitation Erosion Test and quantitative assessment of material resistance to cavitation. *Wear* **1999**, *233–235*, 51–64, doi:10.1016/S0043-1648(99)00195-7.
24. Hattori, S.; Ishikura, R.; Zhang, Q. Construction of database on cavitation erosion and analyses of carbon steel data. *Wear* **2004**, *257*, 1022–1029, doi:10.1016/j.wear.2004.07.002.
25. *ASTM G32 Standard. Test Method for Cavitation Erosion Using Vibratory Apparatus*;
26. Tucker, R. C. *ASM Handbook Volume 5A: Thermal Spray Technology*; 2013 edition.; ASM International, 2013; ISBN 978-1-61503-996-8.
27. Shaw, L. L.; Goberman, D.; Ren, R.; Gell, M.; Jiang, S.; Wang, Y.; Xiao, T. D.; Strutt, P. R. The dependency of microstructure and properties of nanostructured coatings on plasma spray conditions. *Surf. Coat. Technol.* **2000**, *130*, 1–8, doi:10.1016/S0257-8972(00)00673-3.
28. Szala, M. Application of computer image analysis software for determining incubation period of cavitation erosion – preliminary results. *ITM Web Conf.* **2017**, *15*, 06003, doi:10.1051/itmconf/20171506003.

29. Dybowski, B.; Szala, M.; Hejwowski, T. J.; Kiełbus, A. Microstructural phenomena occurring during early stages of cavitation erosion of Al-Si aluminium casting alloys. *Solid State Phenom.* **2015**, *227*, 255–258, doi:10.4028/www.scientific.net/SSP.227.255.
30. Tomlinson, W. J.; Kalitsounakis, N.; Vekinis, G. Cavitation erosion of aluminas. *Ceram. Int.* **1999**, *25*, 331–338, doi:10.1016/S0272-8842(98)00043-1.